UC Irvine

UC Irvine Previously Published Works

Title

Recapitulating the human tumor microenvironment: Colon tumor-derived extracellular matrix promotes angiogenesis and tumor cell growth

Permalink

https://escholarship.org/uc/item/9bq4n172

Authors

Romero-López, Mónica
Trinh, Andrew L
Sobrino, Agua
et al.

Publication Date

2017-02-01

DOI

10.1016/j.biomaterials.2016.11.034

Copyright Information

This work is made available under the terms of a Creative Commons Attribution License, available at https://creativecommons.org/licenses/by/4.0/

Peer reviewed

eScholarship.org Powered by the California Digital Library
University of California

Author Manuscript

Author Manuscript

Author Manuscript

Author Manuscript

HHS Public Access

Author manuscript

Biomaterials. Author manuscript; available in PMC 2018 February 01.

Published in final edited form as:

Biomaterials. 2017 February ; 116: 118–129. doi:10.1016/j.biomaterials.2016.11.034.

Recapitulating the human tumor microenvironment: colon tumor-derived extracellular matrix promotes angiogenesis and tumor cell growth

Mónica Romero-López, PhD[1], **Andrew L. Trinh, BS**[1], **Agua Sobrino, PhD**[1], **Michaela M. S. Hatch, BS**[2], **Mark T. Keating, BS**[1], **Cristhian Fimbres, BS**[1], **David E. Lewis**[2], **Paul D. Gershon, PhD**[2], **Elliot L. Botvinick, PhD**[1,3], **Michelle Digman, PhD**[1], **John S. Lowengrub, PhD**[1,4], and **Christopher C. W. Hughes, PhD**[*,1,2,3]

[1]Department of Biomedical Engineering, The Henry Samueli School of Engineering, UC Irvine

[2]Department of Molecular Biology and Biochemistry, School of Biological Sciences, UC Irvine

[3]The Edwards Lifesciences Center for Advanced Cardiovascular Technology, UC Irvine

[4]Department of Mathematics, School of Physical Sciences, UC Irvine

Abstract

Extracellular matrix (ECM) is an essential and dynamic component of all tissues and directly affects cellular behavior by providing both mechanical and biochemical signaling cues. Changes in ECM can alter tissue homeostasis, potentially leading to promotion of cellular transformation and the generation of tumors. Therefore, understanding ECM compositional changes during cancer progression is vital to the development of targeted treatments. Previous efforts to reproduce the native 3D cellular microenvironment have utilized protein gels and scaffolds that incompletely recapitulate the complexity of native tissues. Here, we address this problem by extracting and comparing ECM from normal human colon and colon tumor that had metastasized to liver. We found differences in protein composition and stiffness, and observed significant differences in vascular network formation and tumor growth in each of the reconstituted matrices, both *in vitro* and *in vivo*. We studied free/bound ratios of NADH in the tumor and endothelial cells using Fluorescence Lifetime Imaging Microscopy as a surrogate for the metabolic state of the cells. We observed that cells seeded in tumor ECM had higher relative levels of free NADH, consistent with a higher glycolytic rate, than those seeded in normal ECM. These results demonstrate that the ECM plays an important role in the growth of cancer cells and their associated vasculature.

[*] Fax: (949) 824 8551µ, cchughes@uci.edu.

Publisher's Disclaimer: This is a PDF file of an unedited manuscript that has been accepted for publication. As a service to our customers we are providing this early version of the manuscript. The manuscript will undergo copyediting, typesetting, and review of the resulting proof before it is published in its final citable form. Please note that during the production process errors may be discovered which could affect the content, and all legal disclaimers that apply to the journal pertain.

Conflicts of interest: none

Contributions

MRL, CCWH and JSL conceived the project, interpreted data and wrote the manuscript. AT performed experiments, analyzed the microscopy data and contributed to the manuscript; MD developed the FLIM phasor approach and interpreted data. AS interpreted data and contributed to the manuscript. MMSH performed the *in vivo* experiments and interpreted data. MTK and ELB developed the AMR platform, performed AMR experiments and analyzed the data. CF and DEL contributed to protocol design and performed experiments. PDG performed the mass spectrometry analysis and interpreted data. All authors read and approved the manuscript.

Author Manuscript Author Manuscript Author Manuscript Author Manuscript

Introduction

The extracellular matrix (ECM) is a complex network of proteins and glycosaminoglycans that provides biochemical and biomechanical signaling cues to the cells it surrounds. ECM disruptions can occur in the physical (porosity, fiber orientation), biochemical (composition and growth factor binding capacity), and biomechanical (stiffness) properties of the ECM, and some of these properties help to regulate cell differentiation, adhesion, survival, migration and proliferation rates [1].

There is a growing interest in the study of tumor cell-matrix interactions as these may contribute to cancer development by promoting cell dedifferentiation and cancer stem cell division. For example, the development of tumors has been linked to the desmoplastic reaction [2] which includes the production of large amounts of ECM by myofibroblasts, often in response to inflammation, leading to dramatic tissue remodeling. In response to tumor-derived signals, stromal cells express numerous ECM components, including collagens (I, III, IV, V, XII), proteoglycans and hyaluronan, which help create a more permissive environment for cancer propagation [3]. As a result of these changes in the ECM, the fiber conformation is modified as well as the tumor tissue stiffness [4]. Evidence suggests that these ECM changes can alter tumor growth and differentiation [5]. In particular, collagen can enhance cell proliferation and migration and, as a result, promote cancer cell proliferation [6].

Both *in vivo* and *in vitro* approaches have been used to study the process of cancer progression. *In vivo* tumor models are ideal as they more closely reproduce the native evolution of cancer and its microenvironment. However, it is difficult to control the environment in these models, and visualization of cell-cell and cell-ECM interactions, and quantification of results is problematic without specific imaging technology [7]. In contrast, *in vitro* models are easier to manipulate, offering the opportunity to probe key biological features of several of the stages of cancer progression. However, 2D monolayer cultures have predominated and these fail to model key aspects of the tumor microenvironment, including 3D geometry, porosity, density of ECM binding sites, ECM heterogeneity, and gradients of biochemical factors, among others.

Angiogenesis – the formation of new blood vessels from pre-existing vessels – is a critical feature of solid tumor growth that cannot be reproduced in a 2D environment. Without its own vasculature a tumor cannot grow beyond a few millimeters in size [8]. The angiogenic process starts when tumor cells become hypoxic and those cells and stromal cells (e.g. fibroblasts) secrete diffusible chemical signals, collectively called angiogenic factors. This process activates the expression of matrix metalloproteinases (MMPs) by endothelial cells, enabling their migration away from the parent vessel as a new sprout. ECM morphology and fiber orientation have strong effects on EC migration, sprout extension rate and vascular characteristics [9].

It is now well established that 3D *in vitro* experiments provide a better approximation of the *in vivo* tumor cell microenvironment than do 2D cultures. It has been shown that cancer cell

Author Manuscript Author Manuscript Author Manuscript Author Manuscript

morphology [10], cell migration [11], cell proliferation rates [12] and gene expression [13] are all different in 2D versus 3D cultures. In particular, 3D *in vitro* experiments of tumor spheroids showed upregulated expression of angiogenic factors compared to cells seeded in 2D [14], while other work demonstrated that cells in a 2D environment have lower IC_{50} to drugs for tumor cells than cells in 3D [15]. Finally, it is well known, from the results of Bissell and collaborators, that tumor cells de-differentiate when cultured in 2D, whereas in 3D cultures they adopt morphologies similar to the ones seen *in vivo* [5, 16]. These are just some examples of the importance of studying tumor cells in the correct context.

Recent work looking at tumor cells in a 3D setting *in vitro* have focused on tumor cells or tumor spheroids, grown in Matrigel, collagen or fibrin [17, 18]. Matrigel is highly enriched for laminin 111, but lacks the substantial amounts of collagen normally seen in tumor matrix [19]. Collagen and fibrin, while effective *in vitro* matrices, do not capture the complexity of native matrix. Recent advances in 3D matrices for cell culture include artificial hydrogel systems (e.g. cross-linked peptide-based gels) [20], tissue extracted ECM gels [21], and cell derived matrices [22]. Importantly, hydrogels containing ECM extracted from tissues using decellularization techniques contain almost all of the protein of native tissues and in the correct protein ratios. Furthermore, these gels allow for other tunable features such as rheological properties and fiber density, [23]. Additionally, through polymerization, these gels form three-dimension scaffolds similar to collagen and fibrin gels [21].

Here, we have focused on colorectal cancer (CRC) as a model system as it is the world's fourth most deadly cancer and every year in America 150,000 people are diagnosed with CRC, and 50,000 die of the disease. We have previously published on the importance of the 3D microenvironment when studying CRC drug responses [24] and we extend those studies here. Specifically, we tested the hypothesis that normal and tumor ECM affect both blood vessel and tumor growth and that this can be recapitulated using reconstituted ECM. We focused on reproducing the native ECM microenvironment by decellularizing, both normal and tumor tissues for incorporation into 3D hydrogels. We found that normal (n)ECM and tumor (t)ECM have different protein compositions, and that significant differences in vascular characteristics and tumor growth are seen in the different matrices. Additionally, using Fluorescence Lifetime Imaging Microscopy (FLIM), we noted a dramatic shift to a more glycolytic metabolism in tumor cells growing in tECM versus nECM.

Materials and Methods

Materials, cells and animals

Endothelial growth medium-2 (EGM-2) was obtained from Lonza (Basel, Switzerland), DMEM was from Corning (Corning, New York), Fetal Bovine Serum (FBS) was from Gemini Bio Products (Sacramento, California). Sodium deoxycholate (SDC), Triton-X100 and pepsin were from Sigma-Aldrich (St. Louis, Missouri), sodium dodecyl sulfate (SDS) was from Bio-Rad (Hercules, California), DNAse was from Worthington (Lakewood, New Jersey), Antibiotic-Antimycotic, 1X and 10X Dulbecco's phosphate buffered saline (DPBS) and Trizol were obtained from Life Technologies (Carlsbad, California). Fibrinogen 90% clottable bovine was from MP Biomedicals (Santa Ana, California), thrombin (1.3 Units/ml) was from Sigma-Aldrich (St. Louis, Missouri) and polydimethylsiloxane (PDMS) was from

Author Manuscript Author Manuscript Author Manuscript Author Manuscript

Dow Corning (Midland, Michigan). Gene primers were synthesized by Integrated DNA Technologies (Coralville, Iowa). Carboyxlated 2 μm beads were purchased from Bangs Laboratories (Fishers, Indiana).

Endothelial colony forming cells (ECFC) were isolated from human umbilical cords obtained from the University of California (UC), Irvine Medical Center, under an approved Institutional Review Board according to [25]. The normal human lung fibroblasts (NHLF) were purchased from Lonza (Basel, Switzerland) and colon tumor cell lines (SW620, SW480, HCT116) were obtained from UC Irvine's Chao Family Comprehensive Cancer Center. ECFC were cultured in EGM-2 and used between passages 4–8. NHLF (used between passages 4–8), SW620, SW480 and HCT116 were cultured in DMEM containing 10% FBS. All cells were cultured at 37 °C, in a 5% CO_2 incubator. The ECFC and cancer cells were transduced with lentivirus expressing mCherry (LeGO-C2 (plasmid # 27339)) or green fluorescent protein (GFP), (LeGO-V2 (plasmid # 27340), from Boris Fehse (Addgene, (Cambridge, Massachusetts)). Human, anonymous, discarded normal colon tissue and tumor tissue were obtained from the Medical Center, UC Irvine, following an Institutional Review Board-approved protocol.

NOD/SCID mice were purchased from Jackson Laboratories (Bar Harbor, Maine). All *in vivo* studies were completed under the approval of the IACUC committee at UC, Irvine. All the animal work was carried out in accordance with the National Institutes of Health guide for the care and use of Laboratory animals (NIH Publications No. 8023, revised 1978).

Human colon submucosa decellularization

Human discarded colon tissue was obtained from the UC Irvine Medical Center and frozen at −80°C for at least 48 hours to induce cell lysis. The tissue was then thawed in sterile ddH_2O for one hour, and the colon submucosa was isolated by mechanically removing the fat, mucosa and the colon muscle layers. The submucosa was cut into small pieces (approximately 3 × 3 μm length) and washed with ddH_2O for 1 hour. The tissue was then washed with 2X phosphate buffered saline (PBS) for 1 hour and then washed with 2% SDC for six days (our previous studies with porcine and human colon submucosa using 1% SDS resulted in low collagen content compared with the 2% SDC-treated (Fig. S1), and recent decellularization studies showed that SDC is preferred for thin tissues because it is less disruptive of the microstructure of the tissue than SDS [26, 27]). The tissue was washed in 1% Triton-X100 for 30 minutes and rinsed in ddH_2O 10 times for 20 minutes each to remove any remaining detergent. This was followed by a wash in 1X PBS with 1% Antibiotic-Antimycotic for 24 hours at 4°C. All washes were performed in a stir plate at 350 rpm.

Human liver metastasis decellularization

Human discarded tumor tissue was obtained from the UC Irvine Medical Center and. similar to colon submucosa decellularization, the tissue was stored at −80°C for at least 48 hours prior to use, then thawed and washed for 1 hour in ddH20. The tissue was then washed with 2X PBS for one hour and washed with 1% SDS for 4 days. After that, it was washed for 30 minutes with 1% Triton-X100, washed in 100U of DNAse for 1 hour and then rinsed with

Author Manuscript Author Manuscript Author Manuscript Author Manuscript

ddH20 water for 20 minutes, 10 times. This was followed by a wash in 1X PBS with 1X Antibiotic-Antimycotic for 24 hours at 4°C. All washes were done on a stir plate at 350 rpm.

Decellularization confirmation

Random decellularized tissue pieces were selected and fixed in 4% paraformaldehyde (PFA). Paraffin embedding and H & E staining was performed by the UC Irvine Pathology Department.

Colon submucosa and tumor ECM gel preparation

Decellularized tissue was frozen in liquid nitrogen and lyophilized for 3 to 4 days until the tissue was completely dry. The tissue was then milled using an ultra-fine cheese grater (milled ECM can be stored at −80 °C up to 6 months). The ECM tissue powder (100 mg) was enzymatically digested by mixing it with 20 mg of pepsin in 10 ml of 0.1 N HCl to a final ECM solution of 10 mg/ml. The ECM solution was diluted in 10X DPBS resulting in a final ECM concentration of 8 mg/ml. Finally, 1N NaOH was added to bring the solution to pH 7.4. All ECM preparations were used within 6 months of initial extraction from tissue.

Vasculogenesis assays in 3D fibrin and ECM gels

A solution of 8 mg/ml of fibrinogen in 1X DPBS was used for both the fibrin and the ECM-fibrin gels. Both normal colon ECM (nECM) and tumor ECM (tECM) gels were made by mixing 37.5 μl (75%) of normal or tumor ECM solution with 12.5 μl (25%) of fibrin (final concentrations: 6mg/mL normal or tumor ECM solution and 2mg/mL fibrin). ECFC were transduced to express mCherry (1×10^6 cells/ml) were co-suspended with 2×10^6 cells/ml NHLF before polymerization. The gel/cell solutions were mixed with 5 μl of thrombin (1.3 Units/ml thrombin), and pipetted into a PDMS ring (8 μm radius and 0.8 μm height) attached to a 6-well glass-bottom plate and incubated at 37°C for 2 hours. Then 3 ml EGM-2 medium was added on top of the gels. The plate was kept in the incubator at 37°C for the duration of the experiment. EGM-2 medium was changed at day 3 and day 5. Microscope images were taken at day 2, 4 and 8. The experiments was performed three independent times in triplicate.

Colon tumor cell growth assay

GFP- transduced SW620 cells were trypsinized, counted, and 2×10^5 cells/ml were resuspended in the nECM or the tECM to a final concentration of 2×10^5 cells/ml. The gel/cell solutions were mixed with 5 μl of thrombin, pipetted into PDMS rings and attached to a 6-well glass-bottom plate (3 gels per well). The gels were incubated at 37°C for 2 hours for polymerization prior to the addition of 3 ml EGM-2 medium on top of the gels. Medium was changed at day 3 and day 5. Tumor growth was measured by assessing GFP intensity using a plate reader on day 2, 4 and 8. The experiment was performed five independent times in triplicate.

Tumor spheroid-angiogenesis assays

NHLF and GFP-transduced SW620 cells were mixed in a solution of DMEM with 10% FBS and 15% methylcellulose at a ratio of 3:1 (NHLF: SW620). Spheroids of 1000 cells were

Author Manuscript Author Manuscript Author Manuscript Author Manuscript

made by pipetting 150 μl of the suspension into each well of a 96-well low attachment plate and incubating for 24 hours at 37°C. Spheroids were harvested into a 1.5 ml Eppendorf tube, and the supernatant was aspirated. Eight spheroids were added to the protein/cell suspension (2×10^6 cells/ml mCherry-labeled ECFC, 2×10^6 cells/ml NHLF) before casting the gels. The protein/cell solutions were mixed with 5 μl of thrombin, pipetted into a PDMS ring and attached to a 6-well glass-bottom plate. The gels were then incubated for 2 hours at 37°C, prior to the addition of EGM-2 medium on top of the gels. Medium was changed at day 3 and day 5. The experiment was performed three independent times in triplicate.

Quantitative RT-PCR

At day 10 of the colon tumor growth assay, the gels were harvested and digested with Trizol following the manufacture's protocol for RNA isolation. RNA was treated with DNAse (TURBO DNA-free kit for 30 minutes.) Then 5 μg of RNA were used for the generation of cDNA with the iScript cDNA Synthesis Kit. qPCR was performed with SYBR green chemistry and the CFX96 qPCR system (Bio-Rad). Primers (Table S1) of the genes Hexokinase 1, Solute Carrier Family/Facilitated Glucose Transporter Member 1 and Pyruvate Dehydrogenase Kinase 1 were used for gene expression analysis. mRNA expression levels were normalized to expression levels in the nECM and the experiment was performed five independent times. The figure shows the fold changes, the standard error of the mean. Statistical significance is shown as $*p<0.05$ and $**p<0.01$.

Collagen fiber visualization through Second Harmonic Generation (SHG)

To visualize the collagen fiber morphology and distribution, second harmonic generation acquisition of the normal colon submucosa and the tumor tissue was performed using the deep imaging via enhanced-photon recovery (DIVER) imaging microscope by the Laboratory of Fluorescence Dynamics (LFD) at UC Irvine [28], before and after decellularization, as well as after digestion. A Ti:Sapphire laser Mai Tai (Spectra Physics, Santa Clara, California) was used for two-photon fluorescence excitation, with a wavelength of 810 nm and an incident power in the sample of 20mW. The signal was collected using a long working distance water objective (LUMPlanFl 40x/0.80 water immersion objective (Olympus, Tokyo, Japan)) with a field of view of 110um. The SHG signal was obtained using a bandpass filter 320–390 nm.

SDS-PAGE

To further characterize the colon and tumor ECM gels, the ECM solutions were separated by SDS-PAGE using a Pre-cast Polyacrylamide gel and stained with Coomassie Brilliant Blue to visualize proteins present in the ECM.

Mechanical analysis of the three-dimensional gels

Optical tweezers-based active microrheology (AMR) was performed in the laboratory of Dr. Botvinick, UC Irvine as previously described by Kotlarchyk et al. [29]. Briefly, carboyxlated 2 μm beads were embedded into both nECM and tECM gels at a final concentration of 0.08% (w/v) prior to polymerization. Gel concentrations were matched to those used in the vasculogenesis assay. Following polymerization and hydration with media, beads within

Author Manuscript Author Manuscript Author Manuscript Author Manuscript

each gel were trapped by a 1064 nm laser and oscillated at frequencies of 10, 20, 50, 75, and 100 Hz at an amplitude of 200 nm. A second stationary 785 nm beam was used to detect the response of the probe bead. From these data the complex shear modulus (G*) is calculated.

NanoLC-MS/MS

Decellularized normal and tumor tissues were treated as described by Fong, et al. [30] except that the resulting peptides from each tissue, after treatment with iodoacetamide and trypsinization as described [31], were subjected to Nanoscale liquid chromatography coupled to tandem mass spectrometry (nanoLC-MS/MS) using an LTQ Velos Pro mass analyzer (Thermo Fisher Scientific). The mass analyzer was connected to a nanoLC-Easy 1000, with peptide separation in an in-house-packed 25 cm × 75 μm ID C18 nanospray tip. Peptides were resolved in segmented solvent gradients running from 6 to 35% Acetonitrile (CH_3CN) in 0.1% formic acid over 135 min. Fourier Transform Mass Spectrometry (FTMS) precursor spectra were acquired at 60,000 resolution, and up to 20 of the most intense ions with charge states of +2 and higher in each precursor spectrum were subjected to rapid collision induced dissociation (CID) fragmentation and ion trap analysis. Spectral data were re-calculated using Mascot Distiller 2.5.0 (Matrix Science, Boston, Massachusetts). The resulting peaklists were searched against SwissProt (July 2014) with *Homo Sapiens* taxonomy along with a database of common contaminants using Mascot Server 2.5.0 (Matrix Science), with Carbamidomethyl (C) and Oxidation (M) as fixed and variable modifications, respectively, and precursor and fragment mass tolerances of 10 ppm and 0.25 Da, respectively. Mascot protein scores were compared between samples using in-house software. All data shown are above the 95% confidence limit.

Vessel quantification

AngioTool (National Cancer Institute) was used to quantify the vasculogenesis assay (vessel area, vessel length, number of branches). The vessel diameter and fractal dimension quantification was performed using the MATLAB (Mathworks, Natick, Massachusetts) subroutine, RAVE, developed by Seaman *et al.* [32].

Imaging

Fluorescence images were collected with an Olympus IX70 inverted microscope with SPOT software (SPOT Imaging, Sterling Heights, Michigan). Confocal images were obtained using an Olympus FluoView FV1000 (Olympus) microscope.

Fluorescence lifetime imaging microscopy (FLIM)

FLIM data was acquired on a Zeiss LSM 710 (Carl Zeiss, Jena, Germany) microscope using an EC Plan-Neofluar 20x/0.50 N.A. objective (Carl Zeiss, Oberkochen, Germany). NADH was excited by an 80MHz Titanium:Sapphire Mai Tai Laser (Spectra-Physics) at 740nm. Tumor spheroids were embedded in nECM and tECM (containing 2×10^6 cells/ml mCherry-labeled ECFC and 2×10^6 cells/ml NHLF). Individual tumor cells on the borders of tumor spheroids close to the vasculature were imaged with a size of 256 × 256 pixels and a scan speed of 25.21 μsec/pixel. 50 frames were collected and integrated for each fluorescence lifetime image. The excitation and emission signals were separated by a 690

Author Manuscript Author Manuscript Author Manuscript Author Manuscript

nm dichroic mirror, and a 460/80 bandpass filter and photomultiplier tube (H7422P-40, Hamamatsu Photonics, Hamamatsu, Japan) were used for detection. Frequency domain FLIM data was acquired by the A320 FastFLIM FLIMbox (ISS, Champaign, Illinois) and analyzed by SimFCS software (LFD, Irvine, California, www.lfd.uci.edu).

Fluorescence lifetime images were analyzed by the phasor approach, as previously described in [33, 34]. Briefly, every pixel of the integrated FLIM image is transformed into a point on the phasor plot. The g and s coordinates in the phasor plot are calculated from the sine and cosine components of the Fourier transform of the fluorescence intensity decay of each pixel in the image. By NADH FLIM phasor analysis, we mapped the free to protein bound NADH distribution in the images, which has been correlated to the metabolic status of the biological sample [34]. Three independent experiments were performed, each in triplicate and nine images were taken per condition in each experiment.

In vivo studies

GFP- transduced SW620 cells were resuspended in 100 μl of nECM or tECM to a final concentration of 3×10^7 cells/ml. Eight ten-week-old NOD/SCID mice were shaven on the lower left and right flanks, just above the hind limbs. The cell/ECM mixture was implanted subcutaneously: cells/nECM on one side and cells/tECM mixture on the other side of each mouse. Mice were measured biweekly for tumor growth. Tumor volume was calculated by the formula $[(\text{Length} \times \text{Width}^2)/2]$. Tumors were allowed to grow for 5 weeks, then the mice were euthanized, and tumors harvested. The tumors were cut in half, and one half of each tumor was fixed in 4% PFA and embedded in paraffin and cut in sections by the Department of Pathology of UC Irvine for immunohistochemistry (IHC) analysis. The other half of each tumor was embedded and frozen in OCT immediately after harvest and 60 μm were prepared for FLIM analysis.

Immunohistochemistry analysis for CD31

Staining and quantification was performed as previously described [35]. In brief, ECFC inside the tumor sections were visualized by staining for CD31+ cells. The total percent vascular density of the tumors was calculated by determining the area of CD31+ cells versus the entire area of the section using ImageJ (National Institutes of Health). The sections were imaged to obtain the vascular density for each tumor.

Statistics

Data are represented as mean +/− standard deviation of three independent experiments, except where otherwise stated. Statistical significance was determined using an unpaired t-test and a 95% confidence interval. Statistical calculations were performed using GraphPad Prism (GraphPad Software, La Jolla, California).

Results

Preparation of extracellular matrix gels

An overview of ECM gel preparation is provided in Fig 1. Previous work has indicated that individual tissues must be treated with unique protocols during the decellularization process

Author Manuscript Author Manuscript Author Manuscript Author Manuscript

to maintain the chemical properties unique to each tissue [36]. We confirmed this as both normal colon and colon tumor tissues required different decellularization protocols. The normal colon tissue was treated with 2% SDC as a less aggressive detergent optimized for thin tissues, while harsher 1% SDS was necessary to decellularize the thick, highly-vascularized tumor tissue. Each protocol was optimized to yield high recovery of constituent proteins, while maintaining fiber structure.

Characterization of normal ECM and tumor ECM

We obtained tumor tissue from colon tumors that had metastasized to liver. Primary colon tumor tissue is very hard to obtain as most primary tumors receive neoadjuvant treatment before surgical removal and are then unsuitable for our use. Regardless, work on ECM proteomics from the Hynes laboratory indicates that ECM from colon metastases in liver is more similar in composition to colon ECM than it is to the liver itself [37].

To confirm that complete decellularization was achieved in colon and tumor tissue, hematoxylin and eosin (H&E) staining was performed (Fig. 2A, 2B). Random sections were chosen and an absence of nucleic acids was observed (Fig. 2C, 2D). The second harmonic signal from the non-centrosymmetric collagen structure was used to visualize the collagen fibers in the colon and tumor tissues before decellularization, and after gel polymerization. The collagen fibers can be visualized in white to light blue (Fig. 2E – H) in the tissues before the decellularization process as well as in the reconstituted gels. SDS-page gels were run for both of the solubilized ECMs, and bands at the molecular weight of collagen I were observed, suggesting the presence of collagen I in our ECMs (Fig. S2).

Normal ECM supports vascular network formation

To determine if nECM was able to support new vessel formation, NHLF and mCherry-ECFC (2×10^6 cells/ml, 1×10^6 cells/ml respectively) were suspended in nECM and in control fibrin gels. After 4 to 8 days extensive formation of lumenized vessels was observed in both the control (fibrin) and nECM gels (Fig. 3A). Several important features of the vascular networks were quantified using Angiotool software (NCI), including total vessel length, vessel area, number of branches and vessel diameter (these characteristics could be also measured throughout a stereological approach, which may give a more detailed quantification, we refer to the reader to [38] for more information about this technique). Although Angiotool was designed to analyze largely 2D networks, it can be used with isotropic 3D networks to make comparisons between samples, in which case the absolute values for vessel lengths will be (equally) underestimated. In the quantification of these parameters, no significant difference was found between the nECM and vascular networks in fibrin, although there was a trend toward greater vascularity in fibrin. Thus, vessels formed in nECM gels were comparable to those formed in fibrin gels (Fig. 3B–E).

Tumor ECM promotes the formation of tumor-like vasculature

In order to examine if the tECM could support the growth of new vessels, we followed the same procedure as for nECM. NHLF and mCherry-ECFC (2×10^6 cells/ml, 1×10^6 cells/ml respectively) were suspended in nECM and tECM and vessel formation was tracked for 8 days (Fig 4A). Again, we quantified several vascular network characteristics, and significant

Author Manuscript Author Manuscript Author Manuscript Author Manuscript

differences between the two conditions were found. Vessel diameter was increased in the vessels grown in tECM (33.92 μm ± 3.71) compared to those in nECM (22.91 μm ± 2.35) (Fig. 4B). Overall, we found greater variability of vessel diameter in the tECM, as indicated by the higher standard error; this is consistent with observations in human patient tumor-vasculature compared to vasculature in matched normal tissues [39]. The fractal dimension, which is a mathematical measure that quantifies the complexity of a network, was also higher in tECM vascular networks (Fig. 4C). Furthermore, total vessel length, vessel area and the number of branches were significantly higher in the tECM when compared to nECM − by almost 2-fold by day 2 (Fig. 4D–F). This last observation also agrees with what has been found *in vivo* in tumor vasculature [32]. Therefore, the vessels grown in tECM mimicked tumor vasculature, both in variability of vessel diameter within the network and fractal dimension.

Normal ECM and Tumor ECM have proteins in common, but tumor ECM has additional components

To determine protein composition of both ECMs, mass spectrometry was performed. Data from the nano-LC MS/MS were depurated with a threshold score and compared between nECMs and tECM. We collected both Mascot and emPAI scores and these showed high concordance (Table 1A, 1B). We identified a number of ECM proteins that were present in both normal and tumor ECM, but at higher levels in the tumor samples. While collagen I was present equally in each sample, collagen IV was over-represented in the tumor, consistent with our sampling only the desmoplastic tissue. Collagens VI and XIV were also increased in the tumor as were Fibrillin, Emilin, Vitronectin and Laminin (γ1) (Table 1A). Interestingly, we also identified several ECM proteins that were only present in the tumor, including Fibronectin, Periostin, Versican, Thrombospondin-2 and Tenascin (Table 1B).

Microrheological measurements of normal ECM and tumor ECM

Active microrheology was used to characterize the storage and loss moduli of both ECMs. At the same component concentrations, both formulations displayed a marked heterogeneity in stiffness at the microscale. On average, the tECM was considerably stiffer with a 3-fold higher Storage Modulus (G’) and a 3.5-fold higher Loss Modulus (G”) (Table 2).

Colon tumor spheroids grow faster in tumor ECM

Colon tumor cells (GFP-labeled SW620) and mCherry-ECFC were incorporated into either nECM or tECM (Fig. 5A). The tumor cells tended to grow more compactly in the nECM (Fig. 5B), whereas they were more diffuse in the tECM (Fig. 5C). Differences in vascular growth have been noted above (Fig. 4). Tumor growth was then followed over time by daily measurement of GFP intensity using a plate reader. By 9 days we saw a significantly faster growth of the tumor cells in tECM compared to those in nECM (Fig. 5D). To test whether this result could be confirmed *in vivo*, we mixed SW620 cells expressing GFP with either nECM or tECM and injected these subcutaneously into immunocompromised mice and examined their subsequent growth. Although there was an early, non-significant increase in growth of cells in the tECM, this difference disappeared at later time points (Fig. S3). It is likely that invading mouse fibroblasts rapidly remodeled the nECM into tumor ECM under

Author Manuscript Author Manuscript Author Manuscript Author Manuscript

the influence of the tumor cells. Interestingly, however, matrix did affect cell metabolism (see below).

Both tumor cells and endothelial cells are more glycolytic in tumor ECM than in normal ECM

FLIM is a label-free imaging modality that can be used to assess free/bound NADH ratios at single pixel resolution. A higher free/bound ratio of NADH has been shown to correlate with a higher level of glycolysis within cells [40]. We first used FLIM to examine the metabolic profile of the SW620 colon cancer cells and the ECFC that comprised the surrounding vasculature in different ECMs *in vitro*. We identified each cell type by its expression of green (tumor) or red (ECFC) fluorescent proteins (Fig. 6A, B) and used this to generate masks for FLIM analysis of the tumor cells (Fig. 6C, D) and the ECFC (Fig. 6E, F). The associated phasor plot is shown in Fig. 6G. We found a higher relative level of free NADH (blue/white) in both the tumor cells and the ECFC when they were embedded in tECM compared to nECM (Fig. 6H, I), consistent with higher levels of glycolysis. This observation is also consistent with previous work in orthotopic colon tumors and their adjacent vessels in mice [34]. Importantly, the effect of tumor matrix on the NADH free/bound ratio was also seen when we used two other colon cancer cell lines, SW480 and HCT116 (Fig. S4). We next extended these studies to tumors *in vivo*. SW620 cells in either nECM or tECM were injected subcutaneously into immunocompromised mice and then harvested after 5 weeks for FLIM analysis. Similar to our *in vitro* findings we saw a strong increase in the free/bound ratio of NADH in tumor cells growing in the tECM compared to the nECM (Fig. 7A–D), again suggesting that these cells are more glycolytic in the tumor matrix microenvironment. The associated phasor plot is shown in Fig. 7E and quantification of the free/bound shift in the cells grown in tECM is shown in Fig. 7F. Interestingly, although we did not see a significant increase in tumor growth when cells were implanted in tECM, we did observe a significant increase in vascular density in the outermost regions (Table 3).

Tumor ECM promotes higher expression of genes associated with glycolysis

To provide further evidence that the nature of the ECM can influence cellular metabolism we examined expression of several genes associated with glycolysis, including the glucose transporter Hexokinase (*HK1*), Solute Carrier Family/Facilitated Glucose Transporter Member 1 (*SLC2A1/GLUT1*), and Pyruvate Dehydrogenase Kinase 1 (*PDK1*). After 10 days of culture, tumor cells seeded in tECM had higher expression of these genes compared to cells in nECM (Fig. 8), consistent with the increase in free NADH seen by FLIM, and in line with the known bias of tumor cells toward aerobic glycolysis versus oxidative phosphorylation – the Warburg Effect [34].

Discussion

Here we have identified an important role of tumor ECM in promoting both increased vascularity of the tumor, and a shift in tumor and vascular metabolism. Our data are consistent with several recent findings and the growing awareness of the important role that ECM plays in defining the tumor microenvironment.

Author Manuscript Author Manuscript Author Manuscript Author Manuscript

Decellularization has recently become a valuable tool to study ECM and its interactions with different cell types, both in the context of biomaterials, and in the field of regenerative medicine. Decellularization has been successfully employed in a variety of human tissues, including trachea [41], adipose tissue [42], and colon (identification of cancer gene promoters) [43]. Importantly, as was found in our study, these different tissues require unique decellularization protocols to preserve the chemical composition of the native tissues. To our knowledge, this is the first time that human normal colon and cancer tissues have been decellularized for 3D ECM-hydrogel studies.

An alternative technique to obtain hydrogels was introduced by Badylak and colleagues [36] where they developed an ECM gel from the decellularized small intestine submucosa by lyophilizing, powderizing and digesting the tissue, resulting in a solution that could be used as an injectable graft. In earlier studies it was found that these gels could be used as an *in vitro* scaffold – a urinary bladder extracted gel supported adhesion and growth of rat aortic smooth muscle cells *in vitro*, for example [21]. Some years later, a porcine liver-derived gel was extracted and used successfully for culturing human hepatocytes *in vitro* [44]. In addition, our laboratory has shown that a heart-extracted scaffold can be used to enhance maturation of pluripotent stem cells into cardiomyocytes [30].

These studies suggest that the complexity and uniqueness of the native ECM is a key feature for the study of not only “normal” cell behavior *in vitro* but also that of tumors. Thus, there is a need for a better tumor-engineered platform to study the interactions of the tumor cells, vasculature and ECM, particularly in light of emerging evidence of the critical role that ECM plays in the tumor microenvironment. For example, this is well documented by Bissell and collaborators for breast tumors [5, 13], where they find that the cell environment can be as important as the cell genotype. Cells sense the ECM through integrins and these signals are transmitted through the cytoskeleton, leading to changes in gene expression and adaptation to the cells’ local environment. Thus, the local microenvironment can drive changes in both gene expression and cell phenotype [16].

Changes in the tumor ECM, such as increased deposition and crosslinking of the collagen fibers, are the result of cross-talk between the tumor cells and the tumor-associated stromal cells [45]. These cells express lysyl oxidase (LOX), which crosslinks collagens and elastin, resulting in increased stiffness [4]. In this study we also observed differences in collagen fiber structure between the normal tissue and the tumor tissue (Fig. 2). We found the collagen fibers in the tumor tissue to be more linearized and aligned in comparison to collagen fibers in nECM, which were curly and anisotropic, as previously described [45]. Our mass spectrometry data revealed further changes in the tECM composition compared to nECM. We noted the presence of several proteins, such as Periostin, Tenascin-C and Fibrinogen, in the tECM that have been directly linked to tumor progression and poor prognosis [46, 47]. Additionally, using active microrheology, we observed changes in stiffness between the two reconstituted hydrogels, the tECM being 3-fold stiffer than the nECM. It has been documented that tumor tissues are stiffer than normal tissues – for example, breast tumor ECM is at least three fold stiffer than normal ECM [48]. It is hypothesized that these changes in the tissue stiffness are the result of excess fiber crosslinking and changes in ECM composition [49].

Author Manuscript Author Manuscript Author Manuscript Author Manuscript

Several groups have studied blood vessel formation or vasculogenesis in different ECM proteins (collagen or fibrin) or in Matrigel [50, 51]. However, our study is the first to show *in vitro* vascularization of a normal human tissue-derived hydrogel (nECM) or a tECM. We observed that nECM supports vessel formation as well as fibrin, which has been widely used for tissue engineering applications such as vascularized tissue grafts [7]. A vascularized platform has numerous applications in the tissue-engineering field, including *in vitro* disease models, *in vitro* drug testing, as well as for *in vivo* tissue regeneration. Moreover, since tumors require new blood vessels *in vivo* to continue growing beyond a certain size, being able to develop a capillary network in a natural hydrogel would allow us to more closely mimic the *in vivo* tumor niche. To this end we developed a vascularized tissue in a human tumor ECM hydrogel. Unfortunately, supply of primary colon tumor tissue is limited as most patients receive neoadjuvant therapy before resection, making the tumors unsuitable for decellularization. We therefore used colon tumors that had metastasized to liver. Importantly, an ECM proteomics study from the Hynes laboratory has shown that ECM from colon liver metastases is more similar in composition to colon ECM than it is to liver ECM [37].

In our study, we found that the capillary networks developed in tECM had similar characteristics to the *in vivo* tumor vasculature including variability in diameter and increased tortuosity. Recent work looking at vasculogenesis in different ECM materials such as collagen or/and fibrin [52], [50] has revealed that at higher concentrations and increased stiffness, the degree of vascularization is decreased and the average vessel diameter is significantly reduced [53]. However, in our studies we have seen an increase in vessel density, sprouting and vessel diameter in tECM, even though this is on average 3-fold stiffer than the nECM. This suggests that differences in ECM composition are also important for regulating vessel formation [9]. From the mass spectrometry analysis, we identified Tenascin-C in the tECM but not nECM. It is known to be abundant in tumor tissues and to have an important role in endothelial proliferation and vessel malformations [54]. ECM proteins can bind to several growth factors, making them available to cells during matrix proteolysis, and these factors can stimulate enhanced vasculogenesis and angiogenesis [55]. In addition to the ECFC, tumor cell growth was also significantly increased in the tECM. This could be due to the mechanical properties of the tECM or to the composition. Tumor cells are known to proliferate and migrate more in stiffer substrates [11].

In order to investigate the correlation between ECM and cellular metabolism we used FLIM of free and bound NADH as a measure of cellular metabolic activity. We found significant differences in cells grown in the two matrices. Specifically the free/bound ratio of NADH was higher in cells in tECM, consistent with higher rates of glycolysis. This is in line with findings in tissue biopsies where the FLIM signature of the cells in tumor tissues indicates that these cells are more glycolytic than cells in normal tissues [4]. Consistent with changes observed by FLIM, we found significant differences in gene expression of the cells seeded in tumor ECM. The up-regulation of GLUT1 and HK1 gene expression in tECM supports the increase in glucose uptake and glycolysis in tECM compared to nECM. The increased expression of PDK1 (a negative regulator of PDH) favors a reduced entry of glucose into the TCA cycle and a reduced rate of oxidative phosphorylation (OxPhos), consistent with the preference of many tumors for aerobic glycolysis over OxPhos. It is now well established that the metabolic properties of tumor cells are different from those of normal cells [56], and

Author Manuscript Author Manuscript Author Manuscript Author Manuscript

although the molecular mechanism is still not well understood, it is well accepted that cancer cells are more dependent on aerobic glycolysis than on glucose oxidation, and this is independent of oxygen availability, a preference known as the Warburg effect [57]. Here we have demonstrated how the tumor microenvironment participates in this malignant phenotype. Our data identify the tumor microenvironment as an important factor in the regulation of tumor cell metabolism, supporting the work of others, and emphasize the possibility of targeting the 3D tumor microenvironment as a way of controlling tumor growth [58, 59].

Conclusions

We have demonstrated that the composition (and possibly stiffness) of the ECM has a dramatic effect on both tumor cells and the vasculature that supports them. Tumor-derived matrix promotes an altered metabolism, shifting cells towards aerobic glycolysis, as well as enhanced tumor cell proliferation. In addition, vascular network formation is profoundly altered, with increased vessel length but also increased vascular heterogeneity. These studies suggest that targeting the tumor ECM may be a useful adjunct to more direct anti-tumor cell therapies.

Supplementary Material

Refer to Web version on PubMed Central for supplementary material.

Acknowledgments

The authors would like to thank to Enrico Gratton, Alexander Dvornikov and UC Irvine's Laboratory for Fluorescence Dynamics [supported by P41-GM103540; P50-GM076516]. This work was supported by: the National Institutes of Health [NIH UH3 TR00048, R01HL60067] (CCWH), [NIH SIG 1S10OD016328] (PDG), [NIH P41-RRO3155] (MD), [NIH EB015890] and [NIH R01HL085339] (ELB and MTK). UCMEXUS-CONACYT doctoral fellowship, Miguel Velez fellowship (MRL). The Samueli Career Development Chair (MD). The National Science Foundation BEST-IGERT [DGE-1144901] (ALT). CCWH and JSL receive support from the Chao Family Comprehensive Cancer Center (CFCCC) through a National Cancer Institute Center Grant [P30A062203]. We also would like to thank to Robert Edwards, the Department of Pathology, UC Irvine for the provided human tissue and to Ashley Fong and Mary Ziegler for all the scientific discussions regarding this project.

References

1. Lu P, Weaver VM, Werb Z. The extracellular matrix: A dynamic niche in cancer progression. The Journal of cell biology. 2012; 196:395–406. [PubMed: 22351925]
2. Butcher DT, Alliston T, Weaver VM. A tense situation: forcing tumour progression. Nature reviews Cancer. 2009; 9:108–122. [PubMed: 19165226]
3. NystrÖM H, Naredi P, Berglund A, Palmqvist R, Tavelin B, Sund M. Liver-metastatic Potential of Colorectal Cancer Is Related to the Stromal Composition of the Tumour. Anticancer Research. 2012; 32:5183–5191. [PubMed: 23225415]
4. Tung JC, Barnes JM, Desai SR, Sistrunk C, Conklin MW, Schedin P, et al. Tumor mechanics and metabolic dysfunction. Free Radic Biol Med. 2015; 79:269–280. [PubMed: 25532934]
5. Petersen OW, Rønnov-Jessen L, Howlett AR, Bissell MJ. Interaction with basement membrane serves to rapidly distinguish growth and differentiation pattern of normal and malignant human breast epithelial cells. Proceedings of the National Academy of Sciences of the United States of America. 1992; 89:9064–9068. [PubMed: 1384042]
6. Pathak A, Kumar S. Transforming potential and matrix stiffness co-regulate confinement sensitivity of tumor cell migration. Integrative Biology. 2013; 5:1067–1075. [PubMed: 23832051]

Author Manuscript Author Manuscript Author Manuscript Author Manuscript

7. White SM, George SC, Choi B. Automated computation of functional vascular density using laser speckle imaging in a rodent window chamber model. Microvascular research. 2011; 82:92–95. [PubMed: 21419785]
8. Folkman J. Tumor Angiogenesis: A Possible Control Point in Tumor Growth. Annals of Internal Medicine. 1975; 82:96–100. [PubMed: 799908]
9. Newman AC, Nakatsu MN, Chou W, Gershon PD, Hughes CCW. The requirement for fibroblasts in angiogenesis: fibroblast-derived matrix proteins are essential for endothelial cell lumen formation. Molecular Biology of the Cell. 2011; 22:3791–3800. [PubMed: 21865599]
10. Baker EL, Bonnecaze RT, Zaman MH. Extracellular matrix stiffness and architecture govern intracellular rheology in cancer. Biophysical journal. 2009; 97:1013–1021. [PubMed: 19686648]
11. Zaman MH. The role of engineering approaches in analysing cancer invasion and metastasis. Nature reviews Cancer. 2013; 13:596–603.
12. Pickl M, Ries CH. Comparison of 3D and 2D tumor models reveals enhanced HER2 activation in 3D associated with an increased response to trastuzumab. Oncogene. 2008; 28:461–468. [PubMed: 18978815]
13. Kenny PA, Lee GY, Myers CA, Neve RM, Semeiks JR, Spellman PT, et al. The morphologies of breast cancer cell lines in three-dimensional assays correlate with their profiles of gene expression. Mol Oncol. 2007; 1:84–96. [PubMed: 18516279]
14. Fischbach C, Kong HJ, Hsiong SX, Evangelista MB, Yuen W, Mooney DJ. Cancer cell angiogenic capability is regulated by 3D culture and integrin engagement. Proceedings of the National Academy of Sciences of the United States of America. 2009; 106:399–404. [PubMed: 19126683]
15. Longati P, Jia X, Eimer J, Wagman A, Witt M-R, Rehnmark S, et al. 3D pancreatic carcinoma spheroids induce a matrix-rich, chemoresistant phenotype offering a better model for drug testing. BMC cancer. 2013; 13:95. [PubMed: 23446043]
16. Bissell MJ, Radisky D. Putting tumors in context. Nature reviews Cancer. 2001; 1:46–54. [PubMed: 11900251]
17. Nyga A, Loizidou M, Emberton M, Cheema U. A novel tissue engineered three-dimensional in vitro colorectal cancer model. Acta biomaterialia. 2013; 9:7917–7926. [PubMed: 23624217]
18. Jayme LH, Sanjeeb KS, Sivakumar V, Sanja D, Jaspreet KV, Tapan KJ, et al. 3-D Tumor Model for In Vitro Evaluation of Anticancer Drugs. Molecular Pharmaceutics. 2008:5.
19. Serebriiskii I, Castello-Cros R, Lamb A, Golemis EA, Cukierman E. Fibroblast-derived 3D matrix differentially regulates the growth and drug-responsiveness of human cancer cells. Matrix Biol. 2008; 27:573–585. [PubMed: 18411046]
20. Almany L, Seliktar D. Biosynthetic hydrogel scaffolds made from fibrinogen and polyethylene glycol for 3D cell cultures. Biomaterials. 2005; 26:2467–2477. [PubMed: 15585249]
21. Freytes DO, Martin J, Velankar SS, Lee AS, Badylak SF. Preparation and rheological characterization of a gel form of the porcine urinary bladder matrix. Biomaterials. 2008; 29:1630–1637. [PubMed: 18201760]
22. Ahlfors J-EW, Billiar KL. Biomechanical and biochemical characteristics of a human fibroblast-produced and remodeled matrix. Biomaterials. 2007; 28:2183–2191. [PubMed: 17280714]
23. Keane TJ, Londono R, Carey RM, Carruthers CA, Reing JE, Dearth CL, et al. Preparation and characterization of a biologic scaffold from esophageal mucosa. Biomaterials. 2013; 34:6729–6737. [PubMed: 23777917]
24. Sobrino A, Phan DTT, Datta R, Wang X, Hachey SJ, Romero-López M, et al. 3D microtumors in vitro supported by perfused vascular networks. Scientific Reports. 2016; 6:31589. [PubMed: 27549930]
25. Melero-Martin JM, Khan ZA, Picard A, Wu X, Paruchuri S, Bischoff J. In vivo vasculogenic potential of human blood-derived endothelial progenitor cells. Blood. 2007; 109:4761. [PubMed: 17327403]
26. Crapo PM, Gilbert TW, Badylak SF. An overview of tissue and whole organ decellularization processes. Biomaterials. 2011; 32:3233–3243. [PubMed: 21296410]
27. Faulk DM, Carruthers CA, Warner HJ, Kramer CR, Reing JE, Zhang L, et al. The effect of detergents on the basement membrane complex of a biologic scaffold material. Acta biomaterialia. 2014; 10:183–193. [PubMed: 24055455]

Author Manuscript Author Manuscript Author Manuscript Author Manuscript

28. Crosignani V, Jahid S, Dvornikov A, Gratton E. Deep tissue imaging by enhanced photon collection. Journal of Innovative Optical Health Sciences. 2014; 07:1450034.
29. Kotlarchyk MA, Shreim SG, Alvarez-Elizondo MB, Estrada LC, Singh R, Valdevit L, et al. Concentration Independent Modulation of Local Micromechanics in a Fibrin Gel. PloS one. 2011; 6:e20201. [PubMed: 21629793]
30. Fong AH, Romero-López M, Heylman CM, Keating M, Tran D, Sobrino A, et al. Three-Dimensional Adult Cardiac Extracellular Matrix Promotes Maturation of Human Induced Pluripotent Stem Cell-Derived Cardiomyocytes. Tissue Engineering Part A. 2016; 22:1016–1025. [PubMed: 27392582]
31. Wisniewski JR, Zougman A, Nagaraj N, Mann M. Universal sample preparation method for proteome analysis. Nature methods. 2009; 6:359–362. [PubMed: 19377485]
32. Seaman ME, Peirce SM, Kelly K. Rapid analysis of vessel elements (RAVE): a tool for studying physiologic, pathologic and tumor angiogenesis. PloS one. 2011; 6:e20807. [PubMed: 21694777]
33. Digman MA, Caiolfa VR, Zamai M, Gratton E. The Phasor Approach to Fluorescence Lifetime Imaging Analysis. Biophysical journal. 2008; 94:L14–L16. [PubMed: 17981902]
34. Pate KT, Stringari C, Sprowl-Tanio S, Wang K, TeSlaa T, Hoverter NP, et al. Wnt signaling directs a metabolic program of glycolysis and angiogenesis in colon cancer. EMBO J. 2014; 33:1454–1473. [PubMed: 24825347]
35. Ziegler ME, Hatch MMS, Wu N, Muawad SA, Hughes CCW. mTORC2 mediates CXCL12-induced angiogenesis. Angiogenesis. 2016:1–13. [PubMed: 26364300]
36. Badylak SF, Freytes DO, Gilbert TW. Extracellular matrix as a biological scaffold material: Structure and function. Acta biomaterialia. 2009; 5:1–13. [PubMed: 18938117]
37. Naba A, Clauser KR, Whittaker CA, Carr SA, Tanabe KK, Hynes RO. Extracellular matrix signatures of human primary metastatic colon cancers and their metastases to liver. BMC cancer. 2014; 14:1–12. [PubMed: 24383403]
38. Dockery P, Fraher J. The quantification of vascular beds: A stereological approach. Experimental and Molecular Pathology. 2007; 82:110–120. [PubMed: 17320863]
39. Mizuno K, Kudo SE, Ohtsuka K, Hamatani S, Wada Y, Inoue H, et al. Narrow-banding images and structures of microvessels of colonic lesions. Dig Dis Sci. 2011; 56:1811–1817. [PubMed: 21188522]
40. Stringari C, Nourse JL, Flanagan LA, Gratton E. Phasor Fluorescence Lifetime Microscopy of Free and Protein-Bound NADH Reveals Neural Stem Cell Differentiation Potential. PloS one. 2012; 7:e48014. [PubMed: 23144844]
41. Baiguera S, Del Gaudio C, Jaus MO, Polizzi L, Gonfiotti A, Comin CE, et al. Long-term changes to in vitro preserved bioengineered human trachea and their implications for decellularized tissues. Biomaterials. 2012; 33:3662–3672. [PubMed: 22349289]
42. Young DA, Ibrahim DO, Hu D, Christman KL. Injectable hydrogel scaffold from decellularized human lipoaspirate. Acta biomaterialia. 2011; 7:1040–1049. [PubMed: 20932943]
43. Chen HJ, Wei Z, Sun J, Bhattacharya A, Savage DJ, Serda R, et al. A recellularized human colon model identifies cancer driver genes. Nat Biotech. 2016; 34:845–851.
44. Sellaro T, Ranade A, Faulk D, McCabe G, Dorko K, Badylak S, et al. Maintenance of human hepatocyte function in vitro by liver-derived extracellular matrix gels. Tissue engineering Part A. 2010; 16:1075–1082. [PubMed: 19845461]
45. Egeblad M, Rasch MG, Weaver VM. Dynamic interplay between the collagen scaffold and tumor evolution. Current opinion in cell biology. 2010; 22:697–706. [PubMed: 20822891]
46. Michaylira CZ, Wong GS, Miller CG, Gutierrez CM, Nakagawa H, Hammond R, et al. Periostin, a cell adhesion molecule, facilitates invasion in the tumor microenvironment and annotates a novel tumor-invasive signature in esophageal cancer. Cancer research. 2010; 70:5281–5292. [PubMed: 20516120]
47. Van Obberghen-Schilling E, Tucker RP, Saupe F, Gasser I, Cseh B, Orend G. Fibronectin and tenascin-C: accomplices in vascular morphogenesis during development and tumor growth. Int J Dev Biol. 2011; 55:511–525. [PubMed: 21769776]
48. Lopez JI, Kang I, You W-K, McDonald DM, Weaver VM. In situ force mapping of mammary gland transformation. Integrative Biology. 2011; 3:910–921. [PubMed: 21842067]

Author Manuscript Author Manuscript Author Manuscript Author Manuscript

49. Plodinec M, Loparic M, Monnier CA. The nanomechanical signature of breast cancer. Nature Nanotechnology. 2012; 7:757–765.
50. Nakatsu, MN.; Hughes, CCW. Methods in Enzymology. Academic Press; 2008. Chapter 4 An Optimized Three-Dimensional In Vitro Model for the Analysis of Angiogenesis; p. 65-82.
51. Ponce, ML. Tube Formation: an In Vitro Matrigel Angiogenesis Assay. In: Murray, C.; Martin, S., editors. Angiogenesis Protocols. Second. Totowa, NJ: Humana Press; 2009. p. 183-188.
52. Koh, W.; Stratman, AN.; Sacharidou, A.; Davis, GE. Methods in Enzymology. Academic Press; 2008. Chapter 5 In Vitro Three Dimensional Collagen Matrix Models of Endothelial Lumen Formation During Vasculogenesis and Angiogenesis; p. 83-101.
53. Bauer AL, Jackson TL, Jiang Y. Topography of Extracellular Matrix Mediates Vascular Morphogenesis and Migration Speeds in Angiogenesis. PLoS Comput Biol. 2009; 5:e1000445. [PubMed: 19629173]
54. Alves TR, da Fonseca ACC, Nunes SS, da Silva AO, Dubois LGF, Faria J, et al. Tenascin-C in the extracellular matrix promotes the selection of highly proliferative and tubulogenesis-defective endothelial cells. Experimental Cell Research. 2011; 317:2073–2085. [PubMed: 21740900]
55. Irvine SM, Cayzer J, Todd EM, Lun S, Floden EW, Negron L, et al. Quantification of in vitro and in vivo angiogenesis stimulated by ovine forestomach matrix biomaterial. Biomaterials. 2011; 32:6351–6361. [PubMed: 21665268]
56. Zhao Y, Butler EB, Tan M. Targeting cellular metabolism to improve cancer therapeutics. Cell Death & Disease. 2013; 4:e532. [PubMed: 23470539]
57. Warburg O. On the Origin of Cancer Cells. Science. 1956; 123:309–314. [PubMed: 13298683]
58. Cairns RA, Harris IS, Mak TW. Regulation of cancer cell metabolism. Nature reviews Cancer. 2011; 11:85–95. [PubMed: 21258394]
59. Serebriiskii I, Castelló-Cros R, Lamb A, Golemis EA, Cukierman E. Fibroblast-derived 3D matrix differentially regulates the growth and drug-responsiveness of human cancer cells. Matrix Biology. 2008; 27:573–585. [PubMed: 18411046]

Author Manuscript Author Manuscript Author Manuscript Author Manuscript

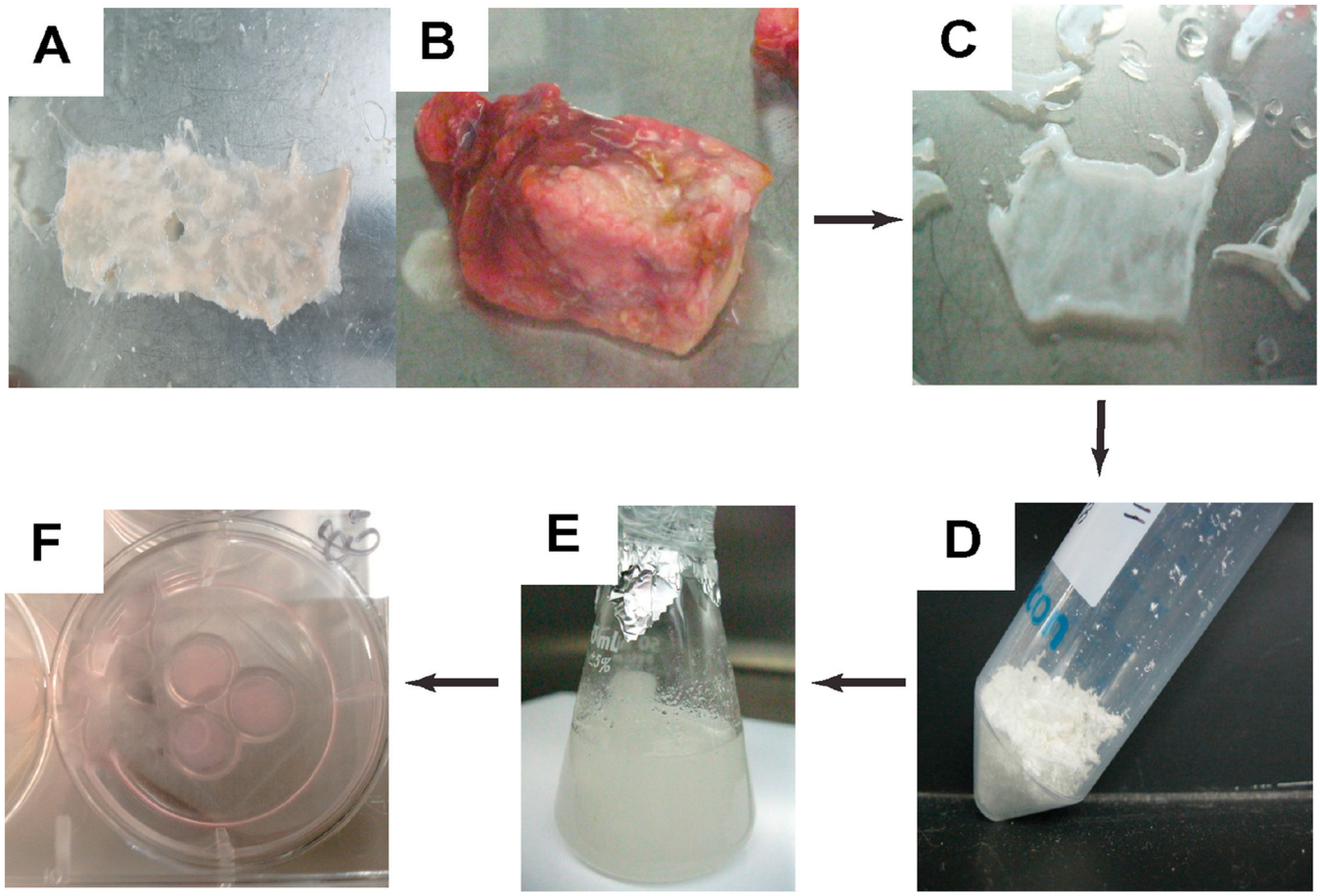

Figure 1. ECM hydrogel extraction process

Fresh human colon tissue (A) or fresh colon tumor metastases (B) were decellularized with the use of several detergents (C), lyophilized and powderized (D), and finally digested with pepsin and HCL (E). The ECM solution polymerizes at 37° C / pH 7.5 forming ECM hydrogels, shown here in PDMS rings (F).

Author Manuscript Author Manuscript Author Manuscript Author Manuscript

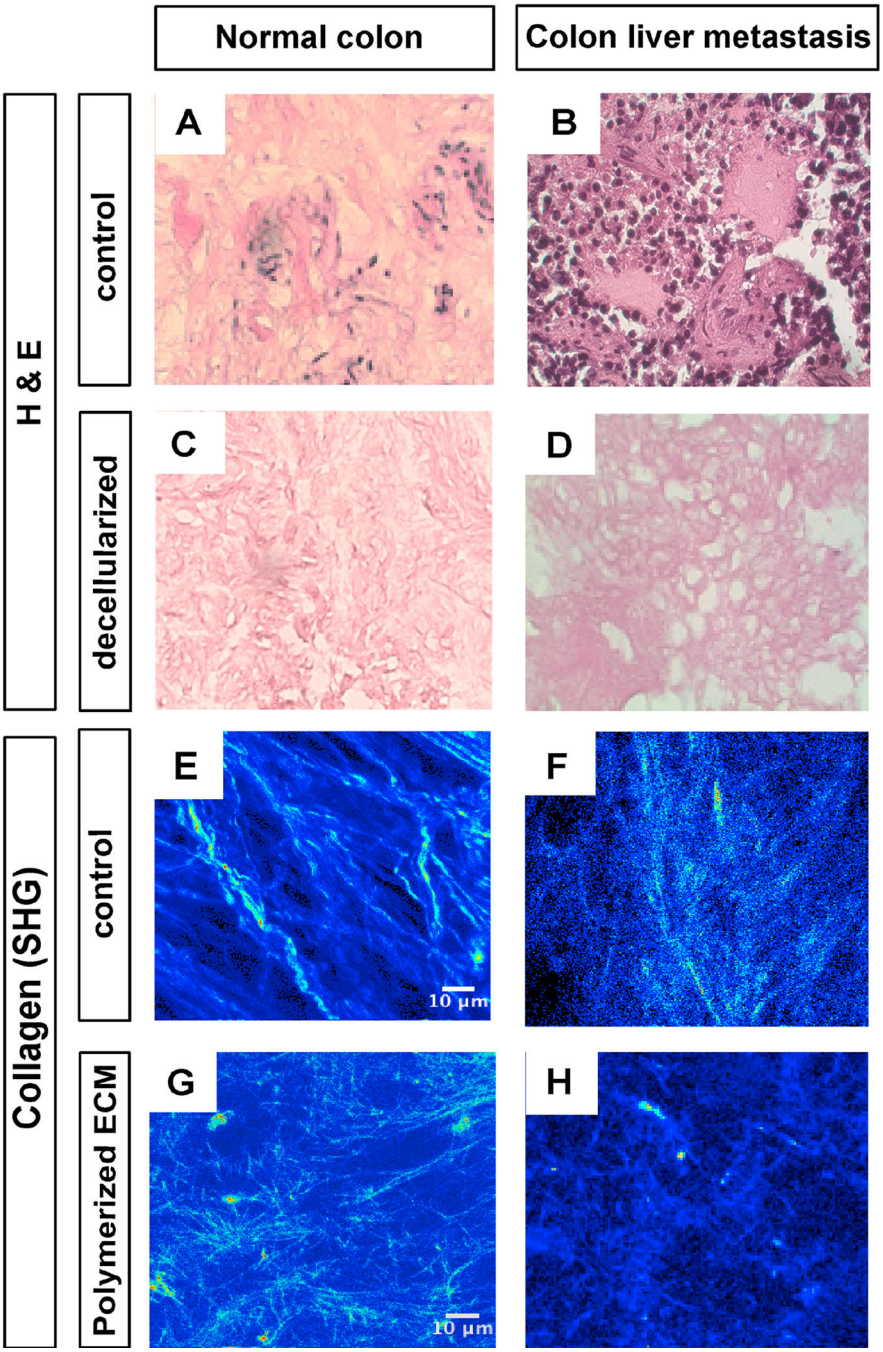

Figure 2. Characterization of the ECM from normal colon and a colon liver metastasis

(A, C, E, G) Normal colon tissue. (B, D, F, H) Colon liver metastasis tissue. (A, B) Tissue before decellularization, H&E stain. (C, D) Tissue after decellularization, H&E stain. Note the lack of nuclei (purple) or debris, indicating complete decellularization. (E, F, G, H) Second harmonic generation (SHG) of collagen fibers (in white to light blue) showing that the collagen is still present after decellularization and polymerization into ECM hydrogels. Scale bar= 10 µm.

Author Manuscript Author Manuscript Author Manuscript Author Manuscript

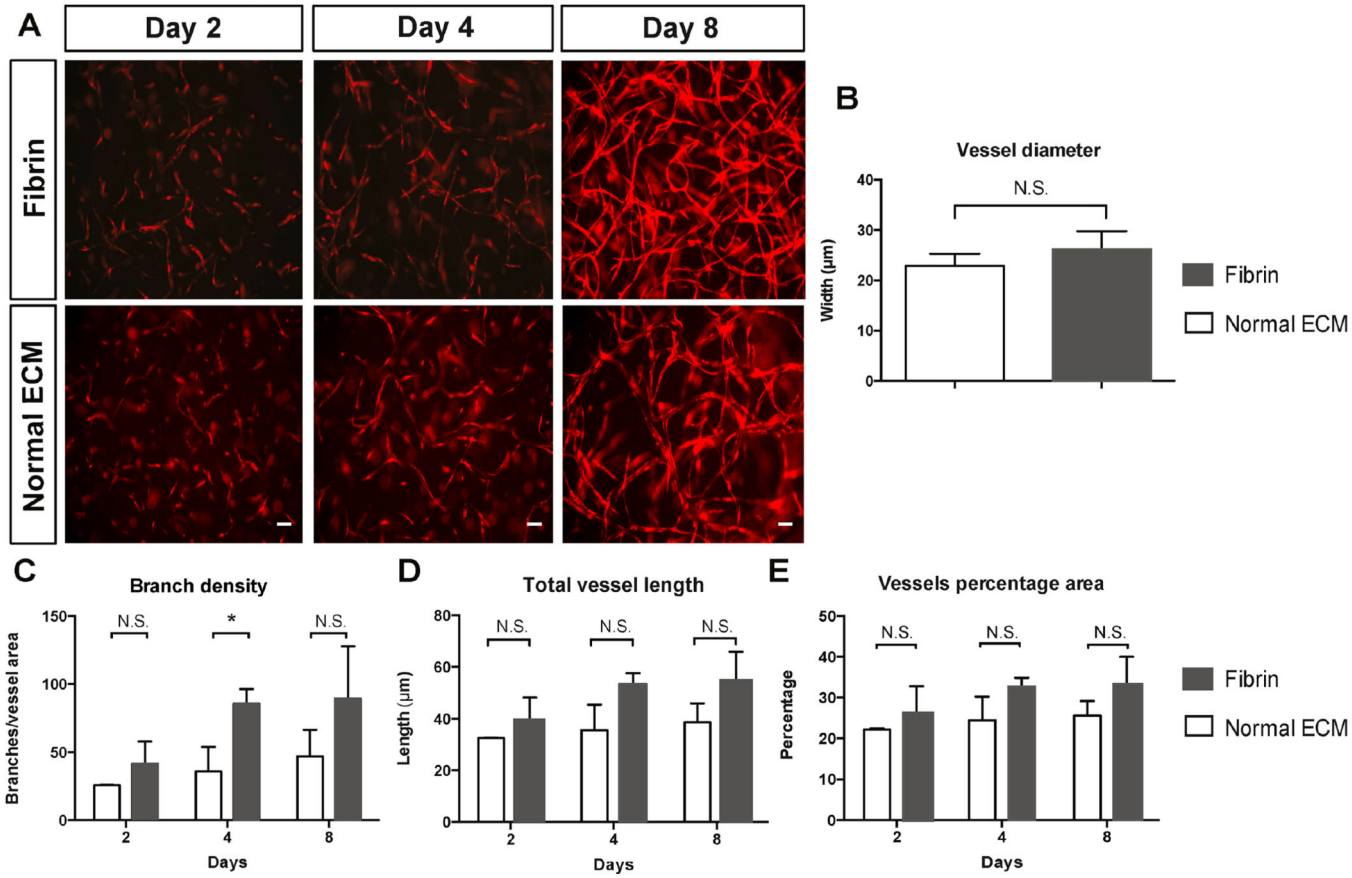

Figure 3. Vasculogenesis assay in Fibrin versus Normal ECM (nECM)

(A) Representative images of cocultured NHLF (1×10^6/ml) and ECFC (2×10^6/ml, mCherry-transduced) in Fibrin (8 mg/ml) and nECM (8 mg/ml) at day 2, 4, and 8. The capillary networks developed over 8 days in Fibrin and nECM. (B) Vessel diameter at day 8 in Fibrin and nECM. No significant differences were evident (N. S.). Branch density (C), total vessel length (D) and vessel percentage area (E) increased over time in both conditions. All quantified parameters were higher in Fibrin than in nECM, however differences were not statistically significant. Data shown are representative of three independent experiments. Error bars are standard deviations. Student t-test, $p>0.05$. Scale bar=100 µm.

Author Manuscript Author Manuscript Author Manuscript Author Manuscript

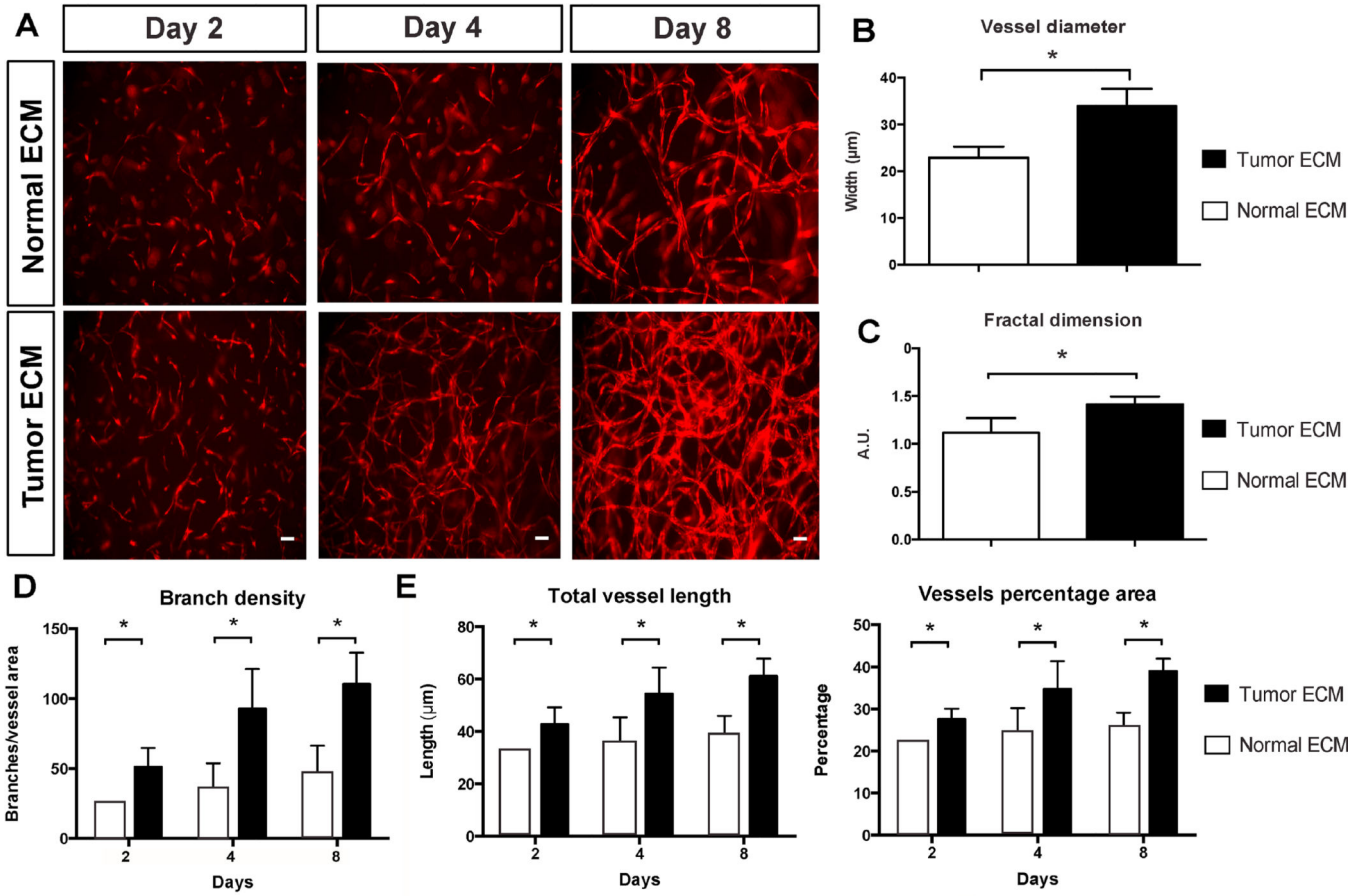

Figure 4. Vasculogenesis assay in Normal ECM (nECM) versus Tumor ECM (tECM)

Representative images of cocultured NHLF (1×10^6/ml) and ECFC (2×10^6/ml, mCherry-transduced) in nECM (8 mg/ml) and tECM (8 mg/ml) at day 2, 4, and 8 (A). The capillary network developed over 8 days in nECM and tECM. (B) Vessels that formed in the tECM displayed significantly larger diameters when compared to those that formed in the nECM at day 8 ($p<0.05$). Additionally, vessels in the tECM were significantly more complex as indicated by increased fractal dimension after 8 days (C) and increased branch density (D). Total vessel length (E) and vessel percentage area (F) were also significantly higher in tECM when compared to nECM. Data shown are representative of three independent experiments. Student's t–test (n=3, *$p<0.05$). Error bars are standard deviations. Scale bar=100 μm.

Author Manuscript Author Manuscript Author Manuscript Author Manuscript

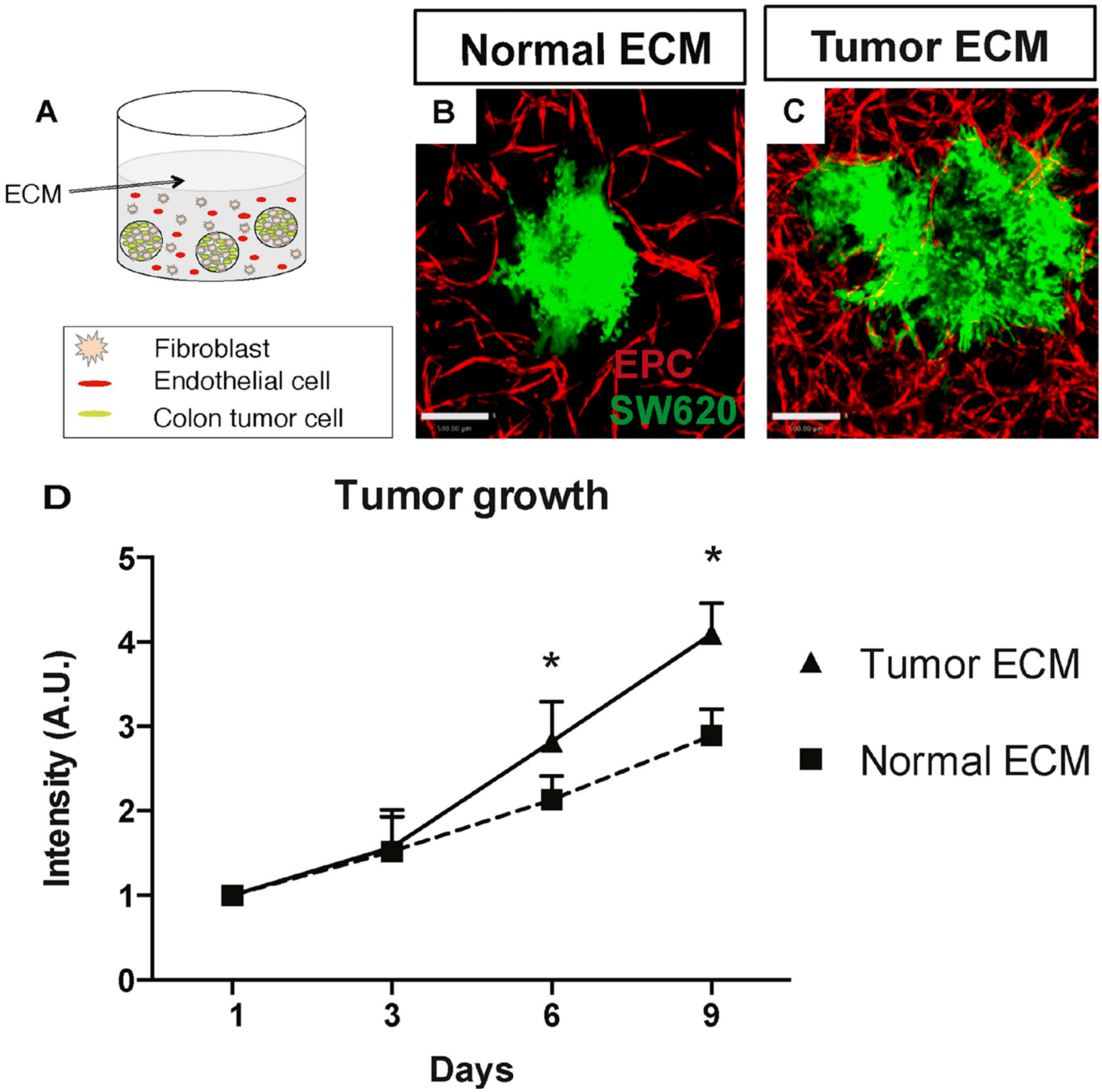

Figure 5. Tumor cell growth is increased in Tumor ECM (tECM)

(A) Coculture of NHLF (1×10^6/ml) and ECFC (2×10^6/ml, mCherry-transduced) with SW620 colon tumor cells (1000 cells/spheroid, GFP-transduced) in nECM (B) and tECM (C) at day 4. (D) SW620 cell (2×10^5/ml) growth was quantified – tumors in tECM grew significantly faster than in nECM. Data shown are representative of five independent experiments. Student's t-test *$p<0.05$. Error bars are standard deviations. Scale bar= 500 μm.

Author Manuscript Author Manuscript Author Manuscript Author Manuscript

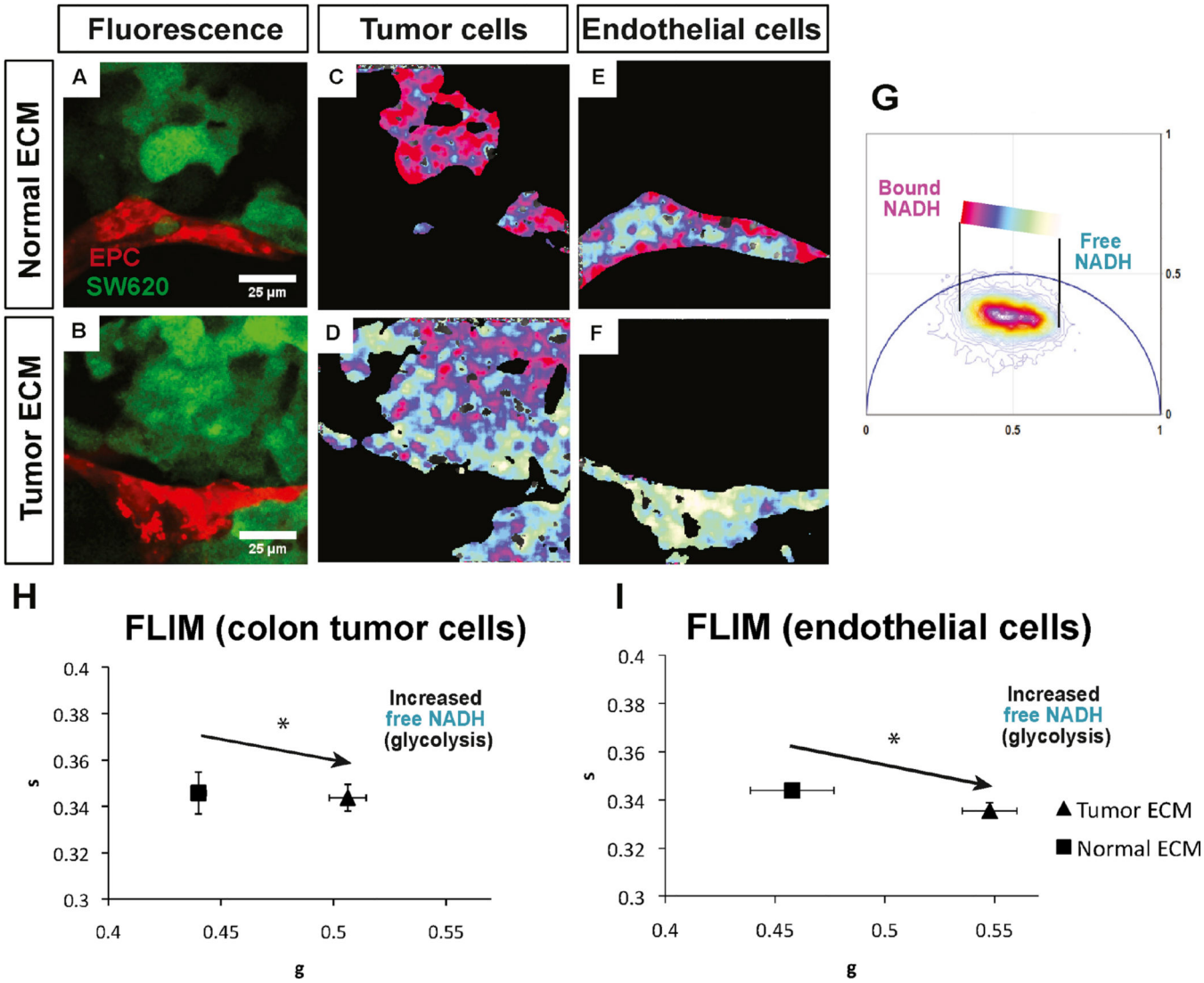

Figure 6. Fluorescence Lifetime Imaging Microscopy *in vitro*

Fluorescence images of ECFC (mCherry) and colon tumor cells SW620 (GFP) in three-dimensional cultures in nECM (A) and tECM (B). Phasor color map of the tumor cells in nECM (C) and tECM (D). Phasor color map of the ECFC in nECM (E) and tECM (F). (G) Phasor histogram of the FLIM images with the color scale representing regions of free and bound NADH. (H) FLIM phasor coordinates for SW620 cells seeded in nECM and tECM. (I) FLIM phasor values for ECFC seeded in nECM and tECM. Data shown are representative of three independent experiments. Student's t-test (n=3, *p<0.05). Error bars are standard deviations. Scale bar = 25 µm.

Author Manuscript Author Manuscript Author Manuscript Author Manuscript

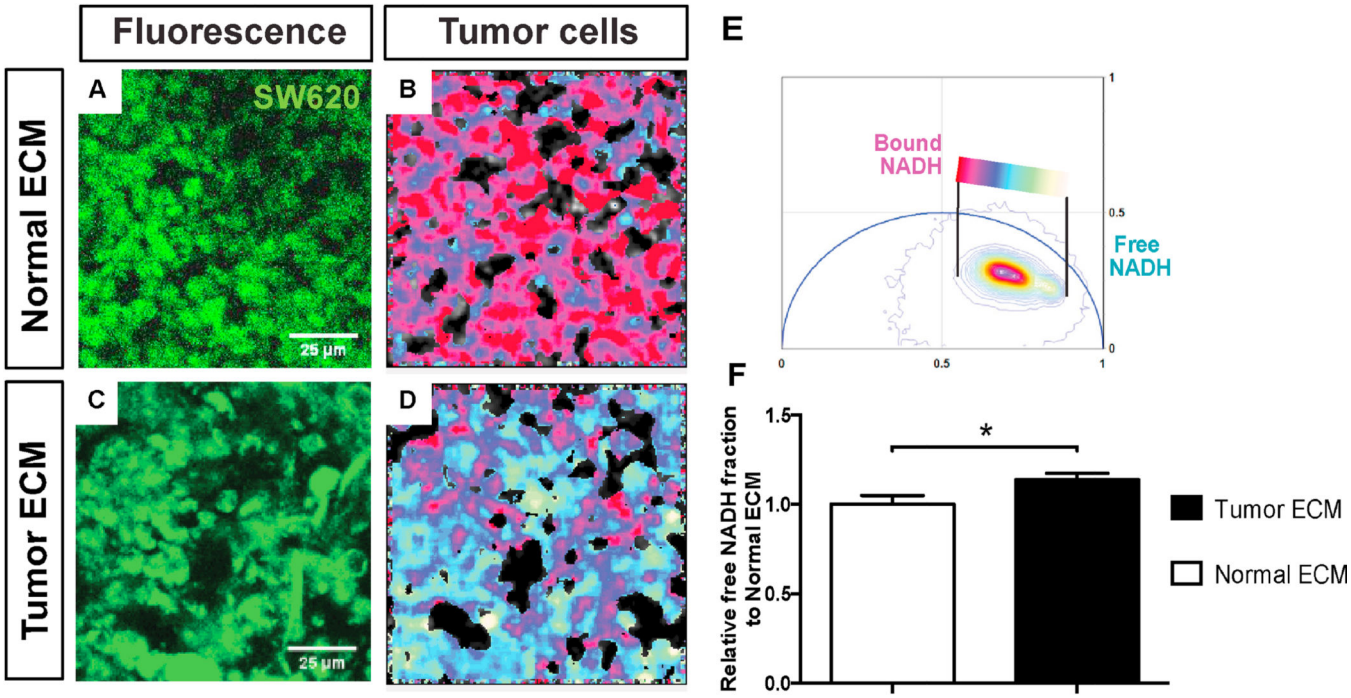

Figure 7. Fluorescence Lifetime Imaging Microscopy *in vivo*

Fluorescence images of subcutaneously-injected colon tumor cells SW620 (GFP) suspended in nECM (A) or tECM (C). Phasor color map of the tumor cells in nECM (B) and tECM (D). (E) Phasor histogram of the FLIM images with the color scale representing regions of free and bound NADH. (F) Relative increase of free-NADH of tumor cells in the tECM. CD31 staining of vessels in a tumor sections in nECM (G) and tECM (H). Vessel percentage area was significantly increased in tumors seeded in tECM (I). Data shown are representative of three independent experiments. Student's t-test *$p<0.05$. Error bars are standard deviations. Scale bars = 25 µm (A–D), 500 µm (G, H).

Author Manuscript Author Manuscript Author Manuscript Author Manuscript

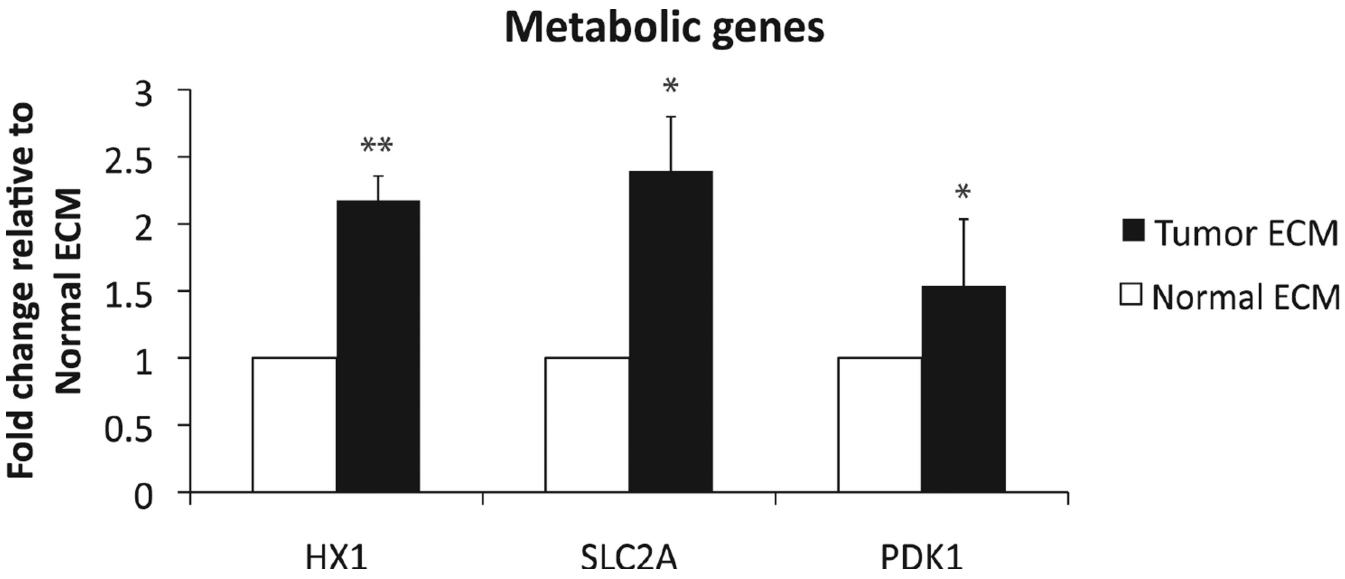

Figure 8. tECM induces up-regulation of genes involved in glycolytic metabolism

Quantitative RT-PCR validation of changes in glycolytic metabolism in colon tumor cells (SW620) seeded in tECM: 1) HX1 (Hexokinase 1); 2) SLC2A (Solute Carrier Family/ Facilitated Glucose Transporter Member 1); and, 3) PDK1 (Pyruvate Dehydrogenase Kinase). Data shown are representative of five independent experiments. Student's t-test (n=5, *p<0.05, **p<0.01). Error bars are standard deviations of the mean.

Author Manuscript Author Manuscript Author Manuscript Author Manuscript

Table 1

Mass spectrometry analysis of normal (nECM) and tumor (tECM) ECM.

A: Differential Mascot scores for ECM proteins			
Gene symbol	**Gene name**	**Relative Mascot score: tumor ECM/normal ECM**	**Relative emPAI score: tumor ECM/normal ECM**
FBN1	Fibrillin	3	2
CO1A1	Collagen I (α1)	1	1
CO1A2	Collagen I (α2)	1	1
CO4A2	Collagen IV (α2)	5	2
CO6A1	Collagen VI (α1)	3	3
CO6A3	Collagen VI (α2)	9	8
COEA1	Collagen XIV (α1)	5	5
VTNC	Vitronectin	4	5
EMIL1	Emilin	9	11
LAMC1	Laminin (γ1)	7	8

B: ECM Proteins present only in Tumor ECM	
Gene symbol	**Gene name**
FINC	Fibronectin
CO6A2	Collagen VI (α2)
COCA1	Collagen XII (α1)
TENA	Tenascin
POSTN	Periostin
CSPG2	Versican
FBLN3	EGF-containing fibulin-like extracellular matrix protein
FBLN4	EGF-containing fibulin-like extracellular matrix protein
BGH3	Transforming growth factor-beta-induced protein ig-h3
PGS1	Biglycan
TSP2	Thrombospondin-2
LAMA2	Laminin (α2)
LAMB1	Laminin (β1)
LAMB3	Laminin (β3)

Proteins present in nECM and tECM with relative Mascot score (column 3) and relative emPAI score (column 4).

Author Manuscript

Author Manuscript

Author Manuscript

Author Manuscript

Table 2

Stiffness of normal (nECM) and tumor (tECM) ECM hydrogels.

Source (3D Hydrogel)	Storage Modulus (G') (Pa)	Loss Modulus (G") (Pa)
Normal ECM	41 ± 29	8.9 ± 5
Tumor ECM	124 ± 54	31 ± 13

Active microrheology was used to determine storage (G') and loss (G") moduli of both hydrogels. For each composition 30 beads were probed and mean ± standard deviation for measurements conducted at 50 Hz are reported.

Author Manuscript

Author Manuscript

Author Manuscript

Author Manuscript

Table 3

Average vessel density percentage of *in vivo* tumor sections.

% Distance from Tumor Edge[1]	Normal ECM[2]	Tumor ECM[2]	p Value
0–20	1.16 ± 0.32	1.83 ± 0.56	<0.05
20–40	0.80 ± 0.23	1.64 ± 0.37	0.058
40–60	0.57 ± 0.06	1.78 ± 0.58	0.056

Vessel percentage area was significantly increased in the outer regions of tumors seeded in tECM. Data shown are representative of three independent experiments.